ORIGINAL RESEARCH ARTICLE

Design and performance evaluation of partial geometry configurations of total-body PET: A Monte Carlo study

Hadi Rezaei[1,2], Peyman Sheikhzadeh[3], Pardis Ghafarian[4,5], Mohammad Reza Ay[1,2]

[1]Department of Medical Physics and Biomedical Engineering, Tehran University of Medical Science, Tehran, Iran

[2]Research Center for Molecular and Cellular Imaging, Tehran University of Medical Sciences, Tehran, Iran

[3]Department of Nuclear Medicine, Imam Khomeini Hospital Complex, Tehran University of Medical Sciences, Tehran, Iran

[4]Chronic Respiratory Diseases Research Center, National Research Institute of Tuberculosis and Lung Diseases, Shahid Beheshti University of Medical Sciences, Tehran, Iran

[5]PET/CT and Cyclotron Center, Masih Daneshvari Hospital, Shahid Beheshti University of Medical Sciences, Tehran, Iran

ARTICLE INFO

*Corresponding Author:
Dr. Mohammad Reza Ay
Address: Department of Medical Physics and Biomedical Engineering, School of Medicine, Tehran University of Medical Sciences, Tehran, Iran
Email: mohammadreza_ay@sina.tums.ac.ir

ABSTRACT

Introduction: This study proposes various designs of partial-ring geometry total-body positron emission tomography (PET) scanners which maintain an extended axial field of view (AFOV) while remaining cost-effective, without sacrificing image quality.

Methods: The total-body uEXPLORER PET scanner was simulated using the GATE Monte Carlo code. Partial-ring PET configurations were simulated, reducing the number of detectors by 25% in both the transaxial and axial directions. The sensitivity, noise equivalent count rate (NECR), and image quality of the partial-ring configurations were compared to those of the full-ring configuration.

Results: The system sensitivity of partial-ring designs was 0.61 and 0.77 times that of the full-ring detector PET for detector reduction in the axial and transaxial directions, respectively. Notably, despite the higher sensitivity, the 10 mm sphere could not be detected in the transaxial reduction mode. When considering all spheres except the 10 mm one, the mean relative error of contrast recovery (CR) for the same time duration was 2% for detector reduction in the axial direction, whereas it increased to 9% for reduction in the transaxial direction.

Conclusion: The results show that reducing the number of detectors in total-body PET scanners can significantly lower manufacturing costs associated with long AFOV PET systems. Although the reduced detector configuration resulted in lower sensitivity, the image quality of the NEMA phantom was found to be superior in the axial reduction mode compared to the transaxial reduction mode. Additionally, the image quality exhibited only a slight difference from that of the full-ring scanner.

INTRODUCTION

In recent years, Positron Emission Tomography (PET) has gained prominence as a gold-standard diagnostic method with diverse applications in oncology, neurology, cardiology, endocrinology, and drug delivery [1-3]. However, current clinical PET scanners typically have a limited axial field of view (AFOV) ranging from 15 to 26 cm [4]. This small AFOV imposes several limitations on imaging capabilities. Firstly, the scanner's sensitivity is compromised, resulting in a lower signal-to-noise ratio (SNR) [5]. Additionally, imaging the entire body simultaneously becomes a challenge, particularly in dynamic imaging scenarios [6]. The use of multi-bed dynamic imaging further prolongs scanning time, leading to patient fatigue, motion artifacts, and reduced radiopharmaceutical activity [7]. Consequently, the development of PET scanners with an extended AFOV holds promise in addressing these issues. The utilization of total-body PET scanners offers several benefits including increased scanner sensitivity, reduced scan time, lower injected patient dose, and improved imaging capabilities for children and pregnant women [8]. Furthermore, total-body PET enables dynamic imaging with a single bed position, providing added advantages [8]. Recognizing these benefits, researchers and designers have focused on developing total-body PET scanners or PETs with a longer axial field of view (AFOV) compared to conventional scanners [9, 10]. Notably, the EXPLORER consortium has successfully constructed two long AFOV PET models. Among them, PennPET, designed and built by researchers at the University of Pennsylvania, features an impressive AFOV of 70 cm. This model employs 3.86×3.86×19 mm3 LYSO detectors and is based on Philips technology [11]. The study utilizes the 194 cm long uEXPLORER PET, which was designed and constructed at the University of California [12]. However, despite the numerous advantages associated with total-body PET scanners, they also pose several challenges. One of the primary challenges hindering the widespread adoption of total-body PET scanners is their high cost, with the detector modules being the most expensive component. Nevertheless, several cost-effective conceptual designs have been proposed to reduce overall costs. These include techniques such as reducing the scintillator thickness [13], employing lower-cost scintillators such as BGO or plastic scintillators [14], and utilizing sparse detector configurations [15, 16]. In this context, several studies have evaluated different sparse detector configurations. For instance, Yamaya et al. [17] simulated an 'open PET' configuration comprising two separated HR+ scanners with an AFOV of W=154 mm and a variable gap between them. They reported that when the gap exceeded W, artifacts were observed on both sides of the open space. Zhang et al. [18] investigated the effect of SiPM detector reduction in the Philips Vereos PET scanner. They showed that by removing 50% of the detectors in the transaxial and axial directions, the sensitivity reduced to 1/4th but didn't have a significant impact on semi-quantitative analysis using conventional image-derived metrics.

Therefore, there is a growing demand for long axial field of view (AFOV) scanners that are cost-effective. In this study, our objective is to simulate the uEXPLORER total-body PET scanner and explore the feasibility of removing a limited number of detector modules to achieve a cost-effective total-body PET scanner. We employ Monte Carlo simulation using GATE to assess the physical performance of the partial detector PET models, by removing the detectors in axial and transaxial directions, based on NEMA NU 2-2018 (National Electric Manufacturers Association 2018) standards. A comparison will be made with the full-ring scanner, and subsequently, the under-sampled emission data will be reconstructed using dedicated algorithms to compensate for the impact of removing certain detector modules.

METHODS

Total-body PET specifications

The PET scanner used in this study is simulated based on the specifications of the uEXPLORER total-body PET scanner. It has a ring diameter of 78.6 cm and an axial field of view (AFOV) of 194 cm. The axial direction consists of 8 units, each with a length of 24 cm and a spacing of 2.6 mm. In each unit, there are 14 blocks in the axial direction and 5 blocks in the trans-axial direction. Within each block, there are 6 crystals in the axial direction and 7 crystals in the trans-axial direction. The crystals used in this scanner are LYSO crystals with dimensions of 2.76×2.76×18.1 mm³. The time coincidence window ranges from 4.5 ns to 6.9 ns, depending on the maximum unit difference. The energy resolution is 11.7%, and the time resolution is 500 ps [12, 19, 20]. Figure 1 illustrates the simulated total-body PET scanner.

In the previous study [21], the uEXPLORER PET scanner was simulated and validated.
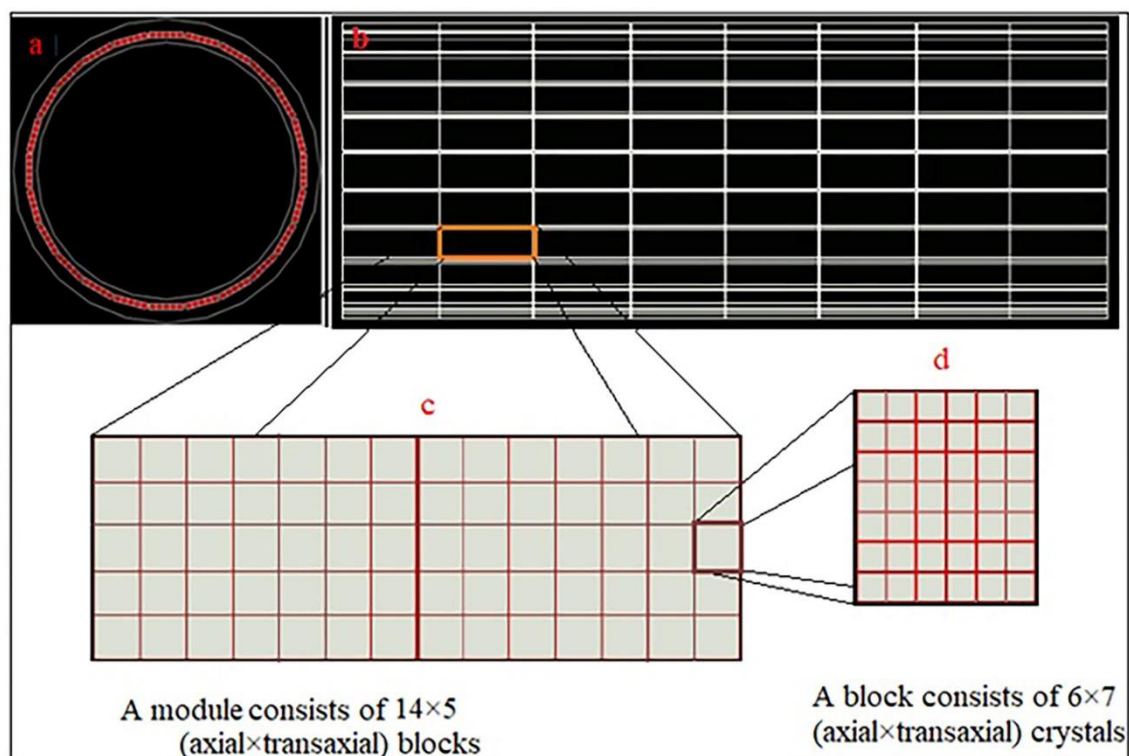
Figure 1. a) Transaxial and b) axial view of the total-body PET simulated consists of c) 14×5 (axial × transaxial) blocks in each module and d) 6×7 (axial × transaxial) crystals in each block

Partial-ring total-body PET simulation

In this study, we conducted simulations for two partial configurations, both involving a proportional reduction in the number of detectors in both the transaxial and axial directions. In the first configuration, we removed two module rings, corresponding to a 25% reduction in the total number of detectors, while maintaining the same axial field of view (AFOV). The second configuration involved the removal of six rows of modules (rsectors) in the transaxial direction. For each configuration, we calculated the system sensitivity, noise equivalent count rate (NECR), and signal-to-noise ratio (SNR) of the image quality phantom. These results were then compared with those obtained from the equivalent full-ring PET scanner, as well as between the two partial configurations.

The simulation of the NEMA image quality phantom was performed with an acquisition time of 120 seconds for each configuration. In a separate evaluation, we extended the simulation time by 50% for the first partial configuration, which involved reducing the number of detector rings in the axial direction. Figure 2 illustrates the two partial total-body configurations, both featuring a 25% reduction in detectors in the axial and transaxial directions.
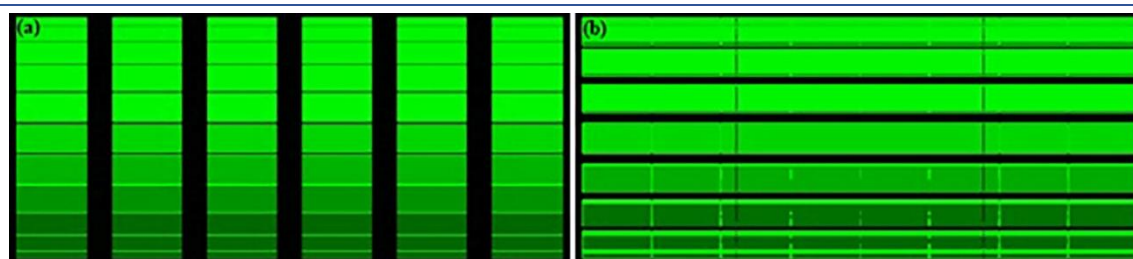

Figure 2. Two partial configurations of total-body PET with a reduction in the number of detectors in the a) axial and b) transaxial directions

Calculation of NEMA parameters

Sensitivity calculation: To calculate the sensitivity, a polyethylene phantom without an aluminum layer was modeled, following the approach outlined by Spencer et al. [19]. The phantom had a length of 1700 mm and a thickness of 2 mm. The sensitivity was specifically calculated at the center of the field of view (FOV)

since this study focuses on comparing the sensitivity between partial-ring scanners and full-ring systems.

Count rates calculations: To assess the count-rate performance, we conducted simulations using an extended phantom that closely resembled the phantom recommended by NEMA. The extended phantom consisted of a 1750-mm long polyethylene cylinder with a diameter of 200 mm. Inside the cylinder, a line source with a length of 1750 mm was positioned within a tube measuring 1750 mm in length and 3.2 mm in diameter. The line source was placed at a radial distance of 45 mm from the center. We calculated the true, scatter, and random rates for the simulated setup. Additionally, we computed the noise equivalent count rate (NECR) using the following equation:

$$NECR = \frac{T^2}{T+S+kR} \qquad (1)$$

Where T, R, and S are the true, random, and scatter coincidences, respectively. The k can be either 1 if the NEC is estimated using a low variance or 2 if delay events are used.

Image quality phantom evaluation: To assess the image quality of total-body PET, we simulated a phantom resembling the NEMA IEC phantom. The simulation involved creating a cylindrical background with a radius of 12.72 cm and a height of 21.4 cm, matching the volume of the IEC phantom. Additionally, we simulated seven spheres within the phantom, each with internal diameters of 10, 13, 17, 22, 28, and 37 mm. These spheres had a glass thickness of 1 mm. The phantom was positioned at the center of the axial field of view (FOV). Both the spheres and the background were filled with F-18, with the background concentration set at 5.1 kBq/cc. The sphere-to-background concentration ratio (SBR) was maintained at 3.7:1. For the simulation acquisition, a total time of 120 seconds was used. The list mode data obtained from the simulation were reconstructed using the OSEM algorithm. The reconstruction parameters included 4 iterations, 20 subsets, and a voxel size of 2.34×2.34×2.34 mm. Furthermore, attenuation, random, and scatter corrections were applied during the reconstruction process.

 Contrast recovery (CR) and signal-to-noise ratio (SNR) were calculated for each sphere as follows [16, 22]:

$$CR_{si} = \frac{\frac{C_{si}}{meanBK_{si}} - 1}{SBR - 1} \qquad (2)$$

$$SNR = \frac{C_{si} - meanBK_{si}}{\sigma BK_{si}} \qquad (3)$$

Where C_{si} is the mean number of counts per sphere, which was measured inside the region of interest (ROI) at the center of each sphere. MeanBK$_{si}$ is the average of all background ROI counts for sphere i with the same diameter as sphere i. σBK$_{si}$ is the average of all background ROI counts and standard deviation for sphere i having diameters of sphere i, respectively. Finally, SBR is the sphere-to-background concentration ratio (3.7:1).

Computing and reconstruction

To perform the simulation and data acquisition, we employed GATE_v9.0 on a cluster. The resulting data and images were analyzed using the ROOT output. For data post-processing, a C++ program was utilized.

Regarding image reconstruction, we employed the Customizable and Advanced Software for Tomographic Reconstruction (CASToR) open-source software [23]. This software provided the necessary tools for reconstructing the images.

RESULTS

In a previous study [21] the sensitivity and NECR parameters of the simulated total-body PET were calculated and compared with experimental results reported by Spencer et al. [19]. The summary of the previous study results is presented here. The simulation study yielded a sensitivity of 144 kcps for the 170 cm phantom at the center of the field of view (FOV). The experimental measurement reported a sensitivity of 147 kcps, resulting in a relative difference of 2% between the experimental and simulated values. This indicates a close agreement between the experimental and simulation results.

The NECR values for the 175 cm extended phantom were 1.902 Mcps at 10 kBq/cc in the simulation and 1.855 Mcps at 9.6 kBq/cc in the experimental measurement. This indicates a relative difference of 2.5% between the experimental and simulation results. The close agreement between the experimental and simulation results demonstrates the accuracy of the simulated total-body PET. These findings affirm the suitability of the simulation model for designing new PET scanner models.

Partial-ring total-body configurations

Table 1 shows the total sensitivity and peak NECR for each partial configuration of the total-body PET and compares them to the equivalent full-ring PET scanner.

Table 1. Comparison of the sensitivity and noise equivalent count rate (NECR) between the partial configurations of total-body PET and the full-ring scanner

System configurations	Sensitivity (kCps/MBq)	Relative sensitivity (partial to full-ring)	NECR (kcps)	Relative NECR (partial to full-ring)
Full-ring	144	1.00	1902	1.00
25% reduction (axial)	88	0.61	970	0.51
25% reduction (transaxial)	111	0.77	965	0.50

Figure 3 shows a transaxial slice through the center of the six spheres and coronal views of the spheres of the simulated image quality phantom produced by the a) full-ring PET scanner (120 s scan duration), b) 25% crystal reduction in the transaxial direction (120 s scan duration), c) 25% crystal reduction in the axial direction (120 s scan duration), and d) 25% crystal reduction in the axial direction (50% increase in scan duration). Table 2 presents the SNR for each configuration, specifically for spheres with diameters of 10, 13, 17, and 22 mm. Figure 4 illustrates the CR of the NEMA IEC phantom across four cases, showcasing the relationship with sphere diameter.
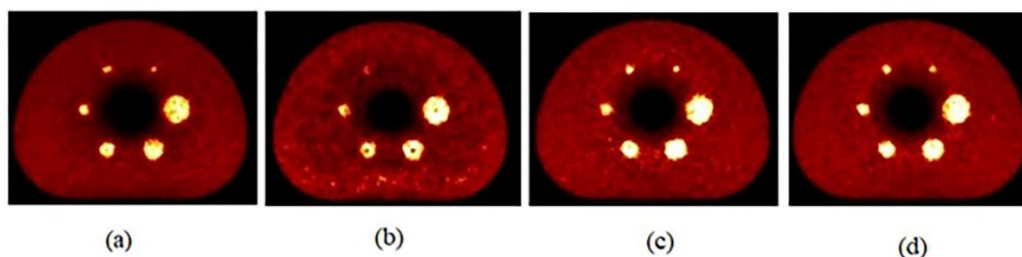

Figure 3. Transaxial slices of the image quality phantom showing: a) full-ring scanner with 120 s scan duration, b) 25% crystal reduction in the transaxial direction with 120 s scan duration, c) 25% crystal reduction in the axial direction with 120 s scan duration, and d) 25% crystal reduction in the axial direction with 180 s scan duration. The images were reconstructed using the OSEM algorithm with 20 subsets and 4 iterations (2.34×2.34 mm^2 pixel size)

Table 2. Signal-to-noise ratio (SNR) for all hot spheres of each scanner configuration and relative difference of the partial scanners results with the full-ring PET scanner

Configuration SD (mm)	Full-ring	A	RDFR (%)	B	RDFR (%)	C	RDFR (%)
10	6.91	0	100	5.11	26.04	5.98	13.45
13	7.04	2.97	57.81	5.63	20.00	6.60	6.25
17	7.71	4.71	38.91	6.32	18.02	6.93	10.11
22	8.38	5.24	37.47	6.96	16.94	8.00	4.53

A: 25% reduction (transaxial 120 s)
B: 25% reduction (axial 120 s)
C: 25% reduction (axial 180 s)
SD: Sphere diameter
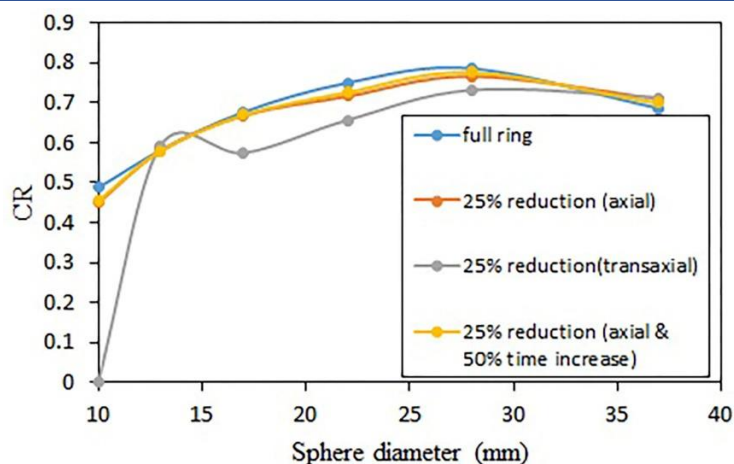RDFR: Relative difference with full-ring

Figure 4. Comparison of contrast recovery (CR) for four cases scanner includes a full-ring scanner, a partial scanner with 25% crystals reduction in the axial direction, a partial scanner with 25% crystals reduction in the transaxial direction, and a partial scanner with 25% crystals reduction in the axial direction and 50% increase in scan duration

DISCUSSION

In recent years, there have been significant endeavors to enhance the sensitivity of clinical PET scanners. One of the most effective strategies to achieve this is by increasing the number of scanner rings. Although PET scanners with long axial field of view (FOV) or total-body PET scanners offer superior sensitivity and image quality compared to current PET systems, their widespread adoption is hindered by the substantial cost of the numerous scintillators required for such scanners. In this study, we focused on simulating the uEXPLORER PET scanner, which represents the first human total-body PET scanner. We successfully validated the simulated scanner by comparing its performance results to the NEMA NU-2 parameters, which are based on measured data. Alongside validating the uEXPLORER total-body PET scanner, we conducted a comprehensive investigation into the influence of various partial-detector designs on the performance of the simulated PET scanner. Specifically, we examined the effects of reducing the number of detectors by the same proportion in both the axial and transaxial directions. Our focus was on assessing the impact of this reduction on key performance metrics, including sensitivity, NECR, and also CR, and, SNR of the image quality phantom. Additionally, we explored the impact of increasing the simulation time by 50% on the CR, and, SNR for one of the partial scanner configurations. Table 1 presents the sensitivity and NECR values for both partial configurations. Interestingly, the NECR remains nearly the same for both partial scanners. However, the sensitivity experiences a further decrease when detectors are removed in the axial direction. Additionally, despite the higher sensitivity observed, the examination of the NEMA image quality phantom demonstrated contrasting outcomes. Figure 3 illustrates that in the NEMA image quality phantom, the transaxial partial scanner (Figure 3b) fails to detect the 10 mm sphere, while the 13 mm sphere is not distinctly visible.

Conversely, in the phantom image of the axial reduction partial-ring scanner, both the 10 mm and 13 mm spheres are distinguishable while under identical conditions (Figure 3c). This can be attributed to improved sampling in this partial scanner configuration. It is important to note that sensitivity refers to a system's ability to convert photons into raw counts and does not directly account for the quality of those counts. Image quality, on the other hand, relies on the quality of the acquired counts, which impacts the discernibility of objects in the image.

The maximum relative difference in contrast recovery between full-ring and partial-ring systems, with a reduction in detectors in the axial direction, was found to be less than 7.8% for a 120 s time duration and 7.0% for a 180 s time duration. On the other hand, when considering the partial-ring system with a reduction in detectors in the transaxial direction (excluding the 10 mm sphere), the maximum relative difference in contrast recovery was less than 15.3%.

The SNR of the spheres was computed for various configurations. The SNR values for spheres in each configuration, along with their relative differences compared to the full-ring scanner are summarized in table 2. As anticipated, the SNR values for the partial scanner constructed by removing detectors in the axial direction are higher compared to the partial model obtained by removing detectors in the transaxial direction. Furthermore, the SNR values for the axial reduction partial scanner are closer to those of the full-ring scanner. The removal of detectors from the PET scanner helps reduce manufacturing costs but also results in a decrease in image quality. However, it is possible to partially compensate for this reduction by increasing the scanning time. Therefore, finding a balance between a slight increase in scanning time and a decrease in the number of detectors can lead to improved results. Table 2 displays the SNR values with a 50% increase in simulation time, demonstrating the impact of this improvement on the SNR. The average relative difference in SNR compared to the full-ring scanner decreases from 20.52% for a 120 s simulation time to 8.58% for a 180 s simulation time. This suggests that the increase in simulation time helps mitigate the degradation in SNR, resulting in improved image quality compared to shorter scan durations.

Hence, by reducing the number of detectors, it is possible to significantly decrease the cost of PET systems without compromising the quality of the resulting images. Considering that the scanning time in total-body PETs is considerably shorter compared to current PETs, it becomes feasible to obtain comparable images to total-body PETs by slightly extending the scanning time using partial total-body PET configurations. Additionally, improving the time-of-flight (TOF) capability of the system can further enhance image quality.

By optimizing and reducing the number of detectors, it is feasible to develop total-body PET scanners at a much lower cost, thereby making these systems more accessible and affordable in

a foreseeable future. This approach allows for the potential realization of cost-effective total-body PET systems while still delivering high-quality imaging capabilities.

One of the limitations of this study is the significant amount of data generated by the long axial field of view (FOV) of the scanner, which resulted in time-consuming processing. Consequently, this limitation prevented us from obtaining high-quality images of the human anthropomorphic phantoms. The extensive data processing requirements together with associated time constraints posed a great challenge in achieving qualitative images for the phantom studies.

CONCLUSION

In this study, we conducted an assessment of the physical performance of partial detector-ring configurations for a total-body PET scanner using Monte Carlo simulations. Specifically, we implemented a reduction of 25% in the number of detectors in both the axial and transaxial directions compared to the current total-body PET configuration. Despite the resulting lower sensitivity, the image quality of the NEMA phantom was proved to be superior in the reduction mode applied in the axial direction compared to the transaxial direction. Furthermore, the image quality of the axial reduction partial scanner showed only a slight difference when compared to the image quality of the full-ring scanner. The utilization of long AFOV PET scanners is on the rise, and there is growing interest among researchers and designers in developing total-body PET systems. In the future, there will likely be much interest on manufacturing total-body PET scanners with reduced number of detectors to make them more cost-effective. If these cost-effective PET scanners can maintain or even enhance image quality, their potential for clinical utilization will significantly increase.

Acknowledgment

REFERENCES

1. Kitson SL, Vincenzo C, Andrea C, Diana S, Luigi M. Clinical applications of positron emission tomography (PET) imaging in medicine: oncology, brain diseases and cardiology. Curr Radiopharm. 2009 Oct 1;2(4):224-53.
2. Ahmed I, Devulapally P. Nuclear medicine PET scan cardiovascular assessment, protocols, and interpretation. Treasure Island (FL): StatPearls Publishing; 2023.
3. Sheikhzadeh P, Ghadiri H, Geramifar P, Ghafarian P, Ay MR. Design and performance evaluation of spheroid geometry for brain PET scanner using Monte Carlo modeling. Iran J Nucl Med. 2019;27(1):32-38.
4. Zhang X, Zhou J, Cherry SR, Badawi RD, Qi J. Quantitative image reconstruction for total-body PET imaging using the 2-meter long EXPLORER scanner. Phys Med Biol. 2017 Mar 21;62(6):2465-85.
5. Cherry SR, Jones T, Karp JS, Qi J, Moses WW, Badawi RD. Total-Body PET: Maximizing Sensitivity to Create New Opportunities for Clinical Research and Patient Care. J Nucl Med. 2018 Jan;59(1):3-12.
6. Cherry SR, Badawi RD, Karp JS, Moses WW, Price P, Jones T. Total-body imaging: Transforming the role of positron emission tomography. Sci Transl Med. 2017 Mar 15;9(381):eaaf6169.
7. Zhang X, Xie Z, Berg E, Judenhofer MS, Liu W, Xu T, Ding Y, Lv Y, Dong Y, Deng Z, Tang S, Shi H, Hu P, Chen S, Bao J, Li H, Zhou J, Wang G, Cherry SR, Badawi RD, Qi J. Total-Body Dynamic Reconstruction and Parametric Imaging on the uEXPLORER. J Nucl Med. 2020 Feb;61(2):285-91.
8. Poon JK, Dahlbom ML, Moses WW, Balakrishnan K, Wang W, Cherry SR, Badawi RD. Optimal whole-body PET scanner configurations for different volumes of LSO scintillator: a simulation study. Phys Med Biol. 2012 Jul 7;57(13):4077-94.
9. Vandenberghe S, Moskal P, Karp JS. State of the art in total body PET. EJNMMI Phys. 2020 May 25;7(1):35.
10. Abstracts of the total body PET conference 2018: Ghent, Belgium. 30 June - 2 July 2018. EJNMMI Phys. 2018 Jun 29;5(Suppl 1):19.
11. Karp JS, Viswanath V, Geagan MJ, Muehllehner G, Pantel AR, Parma MJ, Perkins AE, Schmall JP, Werner ME, Daube-Witherspoon ME. PennPET Explorer: design and preliminary performance of a whole-body imager. J Nucl Med. 2020 Jan;61(1):136-43.
12. Badawi RD, Shi H, Hu P, Chen S, Xu T, Price PM, Ding Y, Spencer BA, Nardo L, Liu W, Bao J, Jones T, Li H, Cherry SR. First human imaging studies with the EXPLORER total-body PET scanner. J Nucl Med. 2019 Mar;60(3):299-303.
13. Surti S, Werner ME, Karp JS. Study of PET scanner designs using clinical metrics to optimize the scanner axial FOV and crystal thickness. Phys Med Biol. 2013 Jun 21;58(12):3995-4012.
14. Moskal P, Salabura P, Silarski M, Smyrski J, Zdebik J, Zieliński M. Novel detector systems for the positron emission tomography. Bio Algoritms Med Syst. 2011 Jun;7(2):73-8.
15. Valiollahzadeh S, Clark JW Jr, Mawlawi O. Using compressive sensing to recover images from PET scanners with partial detector rings. Med Phys. 2015 Jan;42(1):121-33.
16. Zein SA, Karakatsanis NA, Issa M, Haj-Ali AA, Nehmeh SA. Physical performance of a long axial field-of-view PET scanner prototype with sparse rings configuration: A Monte Carlo simulation study. Med Phys. 2020 Apr;47(4):1949-57.
17. Yamaya T, Inaniwa T, Minohara S, Yoshida E, Inadama N, Nishikido F, Shibuya K, Lam CF, Murayama H. A proposal of an open PET geometry. Phys Med Biol. 2008 Feb 7;53(3):757-73.
18. Zhang J, Knopp MI, Knopp MV. Sparse Detector Configuration in SiPM Digital Photon Counting PET: a Feasibility Study. Mol Imaging Biol. 2019 Jun;21(3):447-53.
19. Spencer BA, Berg E, Schmall JP, Omidvari N, Leung EK, Abdelhafez YG, Tang S, Deng Z, Dong Y, Lv Y, Bao J, Liu W, Li H, Jones T, Badawi RD, Cherry SR. Performance Evaluation of the uEXPLORER Total-Body PET/CT Scanner Based on NEMA NU 2-2018 with Additional Tests to

Characterize PET Scanners with a Long Axial Field of View. J Nucl Med. 2021 Jun 1;62(6):861-70.

20. Lv Y, Lv X, Liu W, Judenhofer MS, Zwingenberger A, Wisner E, Berg E, McKenney S, Leung E, Spencer BA, Cherry SR, Badawi RD. Mini EXPLORER II: a prototype high-sensitivity PET/CT scanner for companion animal whole body and human brain scanning. Phys Med Biol. 2019 Mar 21;64(7):075004.

21. Rezaei H, Sheikhzadeh P, Ghafarian P, Zaidi H, Ay MR. Accurate modeling and performance evaluation of a total-body pet scanner using Monte Carlo simulations. Med Phys. 2023 Nov;50(11):6815-27.

22. Salvadori J, Odille F, Verger A, Olivier P, Karcher G, Marie PY, Imbert L. Head-to-head comparison between digital and analog PET of human and phantom images when optimized for maximizing the signal-to-noise ratio from small lesions. EJNMMI Phys. 2020 Feb 21;7(1):11.

23. Merlin T, Stute S, Benoit D, Bert J, Carlier T, Comtat C, Filipovic M, Lamare F, Visvikis D. CASToR: a generic data organization and processing code framework for multi-modal and multi-dimensional tomographic reconstruction. Phys Med Biol. 2018 Sep 10;63(18):185005.